Available online at www.sciencedirect.com
SCIENCE DIRECT®
Bioorganic & Medicinal Chemistry 12 (2004) 2307–2315
Bioorganic & Medicinal Chemistry

A model for identifying HERG K^+ channel blockers ☆

Alex M. Aronov* and Brian B. Goldman

Vertex Pharmaceuticals Inc., Cambridge, MA 02139-4242, USA

Received 17 December 2003; revised 4 February 2004; accepted 5 February 2004

Abstract—Acquired long QT syndrome (LQTS) occurs frequently as a side effect of blockade of cardiac HERG K^+ channels by commonly used medications. A large number of structurally diverse compounds have been shown to inhibit K^+ current through HERG. There is considerable interest in developing in silico tools to filter out potential HERG blockers early in the drug discovery process. We describe a binary classification model that combines a 2D topological similarity filter with a 3D pharmacophore ensemble procedure to discriminate between HERG actives and inactives with an overall accuracy of 82%, with false negative and false positive rates of 29% and 15%, respectively. This model should be generally applicable in virtual library counterscreening against HERG.

1. Introduction

Long QT syndrome (LQTS) is an abnormality of cardiac muscle repolarization that is characterized by the prolongation of the QT interval of the surface electrocardiogram.[1] LQTS is associated with a predisposition for torsades de pointes, a ventricular arrhythmia that can spontaneously degenerate to ventricular fibrillation and cause sudden death.[2] Inherited LQTS is a genetic disease that results from either delayed inactivation of the inward Na^+ channel or a decrease in the current carried by one or more K^+ channels representing gain and loss of function mutations, respectively.[3]

Human ether-a-go-go related gene (HERG) encodes α-subunits that assemble to form pores conducting the rapid delayed rectifier K^+ current (I_{kr}) in the heart.[4,5] This channel contributes to phase 3 repolarization by opposing the depolarizing Ca^{2+} influx during the plateau phase.[3] Over 90 different reported HERG mutations, including deletions, insertions, and missense mutations can cause Type 2 congenital LQTS, primarily by disrupting trafficking of the HERG from the endoplasmic reticulum to the plasma membrane.[6,7]

In recent years, several non-antiarrhythmic drugs have been withdrawn from the market following reports of QT interval prolongation.[3,8] This effect has become a surrogate marker for cardiotoxicity, and has received increasing regulatory attention.[3] HERG has become the focus of many in vitro studies as most of the QT-prolonging drugs have been shown to inhibit I_{kr}.[9,10] Although other potassium currents may also account for a prolongation of cardiac action potential duration, it is HERG K^+ channel blockade that appears to be the major culprit. While HERG inhibition forms the basis for the activity of class III antiarrhythmics, for all other drugs it represents a significant shortcoming.[2,8] Efforts to screen out potential HERG inhibitors early in the development process have generated considerable interest.[9–14]

The molecular basis of HERG channel blockade is not well understood, in large part due to the lack of an experimental atomic resolution structure for the transmembrane complex. The key residues primarily responsible for the high affinity interaction of HERG channels with a number of known ligands, such as cisapride, terfenadine, quinidine, dofetilide, and MK499, were identified by site-directed mutagenesis.[15–17] Two such residues, Y652 and F656, both located in the S6 transmembrane domain, have been shown to be critical in forming the ligand-binding cavity.[15]

Abbreviations: AP, atom pairs; CAT, chemically advanced template; CoMFA, comparative molecular field analysis; HERG, human ether-a-go-go related gene; LQTS, long QT syndrome; PDR, physicians' desk reference; QSAR, quantitative structure–activity relationships; ROC, receiver operating characteristic; TT, topological torsions.

Keywords: HERG; QT prolongation; Binary classification; Pharmacophore ensembles.

☆ Supplementary data associated with this article can be found, in the online version, at doi:10.1016/j.bmc.2004.02.003

* Corresponding author. Tel.: +617-444-6804/6100; fax: +617-444-6566; e-mail: alex_aronov@vrtx.com

0968-0896/$ - see front matter © 2004 Elsevier Ltd. All rights reserved.
doi:10.1016/j.bmc.2004.02.003

Mutagenesis data was corroborated with homology modeling based on the known structure of KcsA, a bacterial K^+ channel.[18] The two aromatic residues were implicated in π-stacking and cation-π interactions with the ligands. In another recent study, Sanguinetti and co-workers showed that positioning of Y652/F656 with respect to the central cavity of the channel was responsible for different sensitivities to drug blockade between HERG and structurally related eag channels.[17] In the absence of a high-resolution structure of the HERG channel, several groups used ligand-based approaches to rationalize the observed structure–activity relationship for HERG inhibition. Ekins et al. derived a HERG pharmacophore model containing four hydrophobic features and one positive ionizable feature using in vitro HERG binding data for a training set of 15 molecules from the literature, and demonstrated its predictive ability on a test set containing 22 molecules.[9] Proposed positive-to-hydrophobe distances were 5.2, 6.2, 6.8, and 7.5 Å. Cavalli et al. constructed a pharmacophore based on an initial set of 31 QT-prolonging drugs for which the HERG K^+ channel blocking activity was measured in transfected mammalian cells.[10] The proposed pharmacophore contained three aromatic moieties connected through a positively charged tertiary amine. Separation of 5.2–9.1, 5.7–7.3, and 4.6–7.6 Å between the nitrogen and the aromatic moieties was proposed.[10] CoMFA analysis was then carried out, and testing was performed by predicting activity of six molecules not included in the training set. Pearlstein and co-workers recently analyzed a set of 32 HERG blockers using CoMSiA.[14] Based on a complementary relationship between CoMSiA results and a homology model of HERG constructed from the crystal structure of the open MthK potassium channel, the authors proposed that the inhibitors bound to HERG orient the ligand long axis along the pore axis, with hydrophobic features located at the intracellular mouth of the channel, and a π-cation interaction with Y652. Buyck et al. recently reported a decision tree-based approach to constructing a HERG binding model using calculated physicochemical descriptors.[11] The final model contained three descriptors—calculated $\log P$ ($C\log P$), calculated molar refractivity, and the pK_a of the most basic nitrogen. The molecules were flagged as HERG ligands if they satisfied the following three conditions:

(i) $C\log P >= 3.7$ (sufficient lipophilicity),
(ii) $-110 =<$ Calculated molar refractivity < 176 (size constraint),
(iii) maximum $pK_a >= 7.3$ (positive charge).

Presence of an acidic functionality and larger topological surface area (TPSA) were proposed as two additional features that favored HERG binding.[11] Similar conclusions were reached by Schneider and co-workers, who developed a QSAR model based on a supervised neural network for classification of HERG channel blockers.[12]

Herein we compare performance of a number of different computational filters for potential HERG inhibitors. In a series of related methods a collection of 2D topological similarity screens was applied to the set of known actives and inactives. Alternatively, an automated pharmacophore ensemble generation procedure was performed using the same training set. In all cases, compound classification is approached in a binary fashion, separating the dataset into actives and inactives based on a chosen threshold. We demonstrate that a combination of these approaches in a 'veto' format (a molecule flagged by either method is considered a potential HERG ligand) provides for an efficient model for rapid screening of large virtual libraries designed to screen out molecules with potential HERG liabilities. The advantages of this approach include ability to rationalize predictions based on structural similarity to, as well as presence or absence of specific pharmacophore features shared by known HERG blockers. To illustrate this, a novel pharmacophore feature is being proposed based on our results to better describe the pharmacophore space associated with a potential to block HERG K^+ channels.

2. Results and discussion

An ensemble pharmacophore model was chosen as the primary screen for HERG channel blockers. The application of 3D pharmacophore descriptors to screening by molecular similarity and binding site complementarity has been reviewed before.[19] Pharmacophore descriptors are generated from conformationally expanded libraries and represent a mapping of standard pharmacophore features and interfeature distances across the conformer library into a single bit string. Ensemble pharmacophore models have been previously applied to lead evolution[20] as well as design of virtual filters.[21] The results for the pharmacophore-based HERG binding model are reported in Table 2. They represent 50 separate cross-validation trials on randomly selected ~20% holdout sets. The best results for these were obtained when using pharmacophore score of 7.5 as a threshold in the classification scheme. The model correctly identified 60% of positives (HERG actives), and 90% of negatives in the training set, resulting in overall accuracy of 84%. When challenged with the holdout set, the model classified 79% of molecules correctly. Nearly half of known actives were pre-

Table 1. Model evaluation criteria

% True positives (sensitivity)	% Predicted HERG actives among HERG actives
% False positives	% Predicted HERG actives among HERG inactives
% True negatives (specificity)	% Predicted HERG inactives among HERG inactives
% False negatives	% Predicted HERG inactives among HERG actives
% PPV (positive predictive value)	% Chance that positive prediction is correct
% NPV (negative predictive value)	% Chance that negative prediction is correct
% Accuracy	% Correct overall predictions

Table 2. HERG dataset classification results[a]

	Sensitivity * 100%[b]	(1-Specificity) * 100%[c]	% Accuracy[d]
VPharm-FP	47 ± 13	13 ± 5	79
TOPO	47 ± 6	9 ± 3	82
AP	47 ± 5	9 ± 3	82
TT	41 ± 18	11 ± 4	79
CATSIM	41 ± 6	9 ± 3	80
VPharm-FP/TOPO	59 ± 6	11 ± 3	83
VPharm-FP/TOPO/AP	71 ± 6	15 ± 5	82
JnJ	18	9	76

[a] Mean and standard deviation presented for 50-fold cross-validation except for the implementation of the HERG model by Buyck et al.[11] (labeled JnJ).
[b] % Predicted HERG actives among HERG actives (% predicted true positives).
[c] % Predicted HERG actives among HERG inactives (% predicted false positives).
[d] % Correct overall predictions.

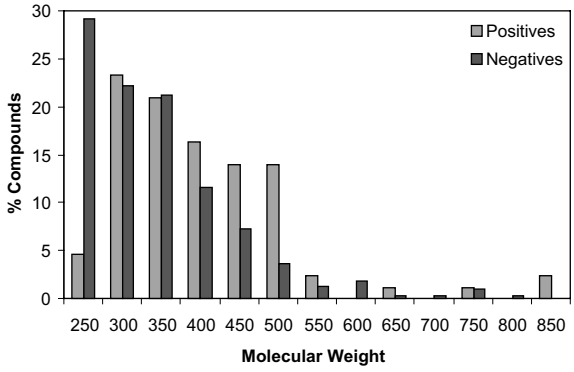

Figure 1. Molecular weight distributions of compounds under study.

dicted to exhibit HERG inhibitory profile, while keeping the false positive rate in check at 13%. The averaged enrichment plots for the holdout set representing 50 cross-validation runs are shown in Figure 3.

We were interested in comparing the performance of the 3D pharmacophore model to a simpler 2D topology-based procedure. We have in the past found the sub-

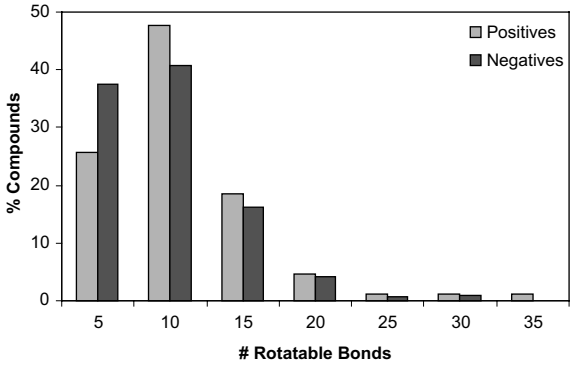

Figure 2. Rotatable bond distributions of compounds under study.

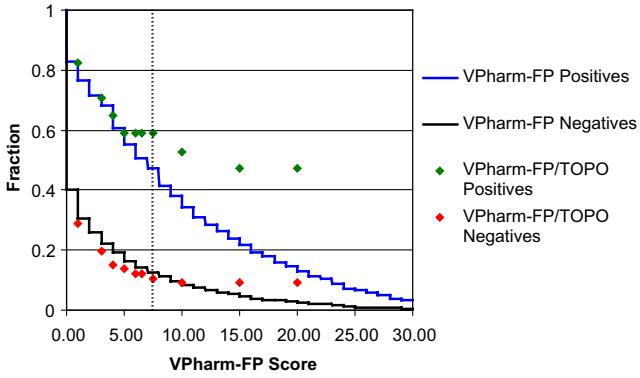

Figure 3. HERG dataset classification using ensemble pharmacophore models. The plot of the fraction of molecules versus ensemble score shows the average results of 50-fold cross-validation. The individual curves depict classification of positive (blue) and negative (black) test sets using VPharm-FP. Also shown are the results of a combined VPharm-FP/TOPO procedure for the positive (green) and negative (red) test sets. Dotted line indicates the optimal Vpharm-FP score cutoff of 7.5. VPharm-FP/TOPO model outperforms VPharm-FP when used alone for HERG dataset classification.

structure descriptors developed at Lederle, topological torsions[22] and atom pairs,[23] useful by enabling to discover active compounds in different chemical classes starting from a probe with an interesting biological activity. Accordingly, these metrics were chosen for evaluation separately, as well as in amalgamated TOPO form (see Methods). A set of five most topologically similar molecules within the test set was generated for every molecule in the holdout set, followed by a vote to determine the outcome of the prediction. This procedure was repeated 50-fold on the cross-validation holdout sets described above. For the TOPO procedure, the overall accuracy in classifying HERG blocking propensity was 82%, with a 47% rate for recovery of HERG actives, and a false positive rate of 9% (Table 2). Similar results were obtained for atom pair scoring, with a false negative rate of 53%, a false positive rate of 9%, and overall classification accuracy of 82%. When topological torsion metric was used for predicting HERG blockade, accuracy declined to 79%, much of it driven by an increase in the rate of false negatives to 59%, while the false positive rate edged up to 11%. A novel 2D metric termed CAT (chemically advanced template search) as published by Schneider et al.[24] at Roche has been proposed to bridge the gap between topological and pharmacophore similarity. Each node in a molecular graph is assigned one of the following generalized atom types: hydrogen bond donor (D), hydrogen bond acceptor (A), positively charged (P), negatively charged (N), or lipophilic (L). Counting pairwise distances up to 10 bonds, each molecule is represented with a 150-dimensional vector. Euclidian distance between vectors can then be used as a similarity metric. When applied to the HERG dataset in the current study, CAT-based classification was accurate 80% of the time, with a false negative rate of 59% and a false positive rate of 9%.

Given the essentially identical performance of the 3D and some of the 2D classification schemes, we wondered

Table 3. Top pharmacophore hypotheses from VPharm-FP

	Pharmacophore nodes			F_1F_2	F_1F_3	F_2F_3
	F_1	F_2	F_3			
1	Pos	Ring	Hyd	4.8–6.7	4.8–6.7	9.3–11.2
2	Pos	Ring	Hyd	4.8–6.7	6.3–8.2	3.3–5.2
3	Acc	Pos	Ring	4.8–6.7	1.8–3.7	6.3–8.2

if using them in combination would lead to improved predictive ability. In order to assess the potential of this approach, we analyzed the lists of true positives identified by the two methods. Interestingly, TOPO voting failed to identify a total of 29 HERG actives, or 34% of the positive dataset in the course of cross-validation. This number was even higher for the ensemble pharmacophore model, with 39 molecules (46%) never classified correctly at the chosen threshold. A comparison of the two incorrectly classified sets revealed that only 19 HERG actives could not be identified by either procedure. In an effort to increase recovery of the positives, the ensemble pharmacophore model was used in combination with the TOPO 2D similarity model in a 'veto' format. In this format, a molecule flagged by either method is considered to be a potential HERG ligand. The performance of the combined VPharm-FP/TOPO model is shown in Figure 3. With a low VPharm-FP cutoff the results approximated those with VPharm-FP alone, while when a high VPharm-FP cutoff was used, performance was identical to that of the TOPO similarity model. However, at the optimal pharmacophore cutoff of 7.5 identified previously, the combined model outperformed either of the two single-component methods, with 41% false negatives, 11% false positives, and an overall accuracy of 83%. Superior predictive power of the combined VPharm-FP/TOPO model in comparison with TOPO or VPharm-FP alone argues that their similar performance based on % recovery of true positives and accuracy (Table 1) appears coincidental.

In an effort to further increase the recovery of true positives in the dataset, we looked into combining the VPharm-FP/TOPO routine with the atom pair scoring in a 'veto' format. Atom pair metric produced superior performance compared to other individual 2D metrics evaluated herein. Indeed, the combined VPharm-FP/TOPO/AP procedure produced a lower false negative rate of 29%, with a false positive rate of 15% and accuracy of 82%. The corresponding positive and negative prediction rates (PPV and NPV, see Table 1) were 52% and 92%, respectively. A ROC curve for this combination scoring procedure is shown in Figure 4.

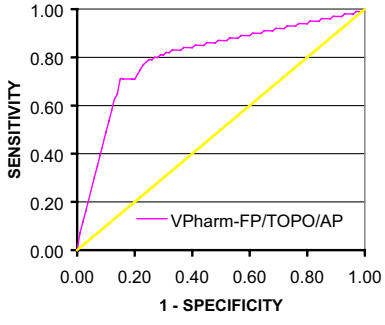

Figure 4. ROC curve for VPharm-FP/TOPO/AP classification combination. The enrichment curve is in magenta. The hypothetical line in yellow is the no-enrichment level.

We were interested in comparing the performance of our HERG classification method to a decision tree-based model by Buyck et al.[11] Rule-based classification produced a large number of false negatives (82%), with a false positive rate similar to our procedures (9%). The overall accuracy was 76%. This result disputes a notion that presence of a basic nitrogen in the molecule along with sufficient hydrophobic character defines the HERG blocking potential of a ligand. While indeed most HERG blockers described to date appear to contain a basic nitrogen functionality, and this fact is reflected in our dataset as well, an even simpler assumption that counting of the basic centers could be used as a quick discrimination model is flawed. For instance, application of this simple rule-based discrimination to our dataset would correctly classify 88% (75 of 85) known HERG actives as active, at the same time labeling 40% (132 of 329) of known HERG inactives as active as well. This approach would be appropriate if one were looking for a set of compounds least likely to inhibit HERG. However, the 40% false positive rate would almost certainly render this simplistic approach undesirable for use as an in silico HERG prioritization filter in a drug discovery program. To be suitable for use as such a filter, the false positive predictions would need to be lower, so as to not stifle creativity on the part of the medicinal chemists, while a lower % recovery of true positives could be tolerated, since any lead hopeful is expected to undergo toxicological profiling, including assays that address the potential for HERG inhibition.

In order to derive structural information from our classification model, the best-performing pharmacophores from VPharm-FP were analyzed. Over the 50 cross-validation runs three hypotheses consistently provided the highest information content for distinguishing HERG actives from inactives. All three were three-point pharmacophores, as shown in Table 3. Hypotheses 1 and 2 represent an extended and a collapsed version of a molecule containing two hydrophobes. Hypothesis 1 is in good agreement with a C0–N–C2 pharmacophore subset by Cavalli et al.[10] (C0—C2 distance range of 10.3–14.7 Å versus our predicted 9.3–11.2 Å). Hypothesis 2 is closest to the C0–N–C1 subset (C0–C1 distance 4.3–6.7 Å versus 3.3–5.2 Å). Interestingly, hypothesis 3 places a hydrogen bond

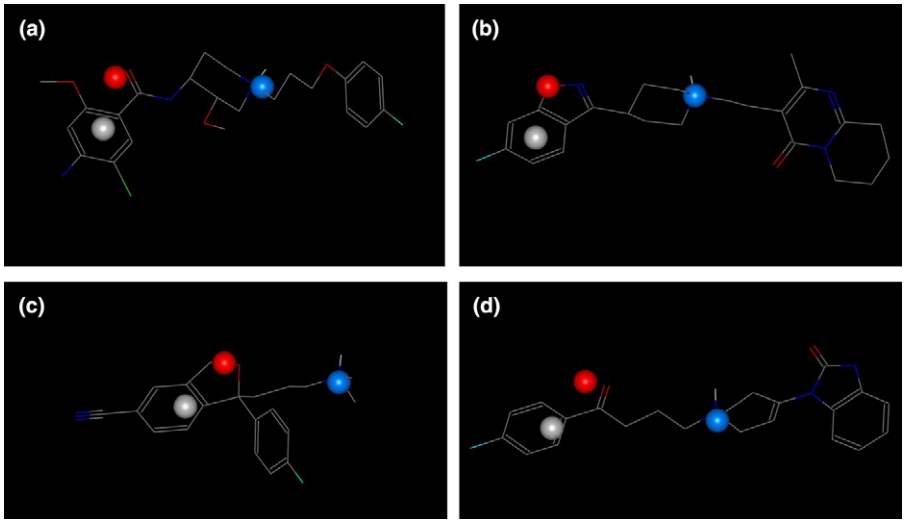

Figure 5. Structures of known HERG blockers fitted to pharmacophore **3**, Table 3. The pharmacophore features are shown with spheres (hydrogen bond acceptor, red; positive charge, blue; ring, gray). Structures are for (a) cisapride, (b) risperidone, (c) citalopram, and (d) droperidol.

acceptor within 1.8–3.7 Å of a centroid of an aromatic ring, implying a spacer comprising one or two bonds. Based on the F_1F_2 and F_2F_3 distances, the acceptor is positioned between the positively charged nitrogen and the aromatic ring. Indeed, a number of known HERG ligands contain an acceptor functionality in a similar arrangement, for example, the amide carbonyl in cisapride, the isoxazole oxygen in risperidone, the ether oxygen in citalopram, or the ketone carbonyl in droperidol (see Fig. 5). Over 28% of the HERG positive dataset contained the aforementioned pharmacophore, compared to under 3% of the compounds in the HERG negative set. While we have not been able to find analog data in the literature that would unequivocally support the role for the hydrogen bond acceptor in HERG binding, it would be of interest to examine this issue further.

Following cross-validation of the VPharm-FP/TOPO/AP model we used an external dataset containing 15 compounds to test its performance. The dataset was assembled from compounds tested internally in a high throughput fluorescence-based assay, and contained eight HERG channel blockers, most of them also confirmed by patch-clamp electrophysiology. The average pairwise Tanimoto similarity between this dataset and the training set of known HERG actives used to construct the model was calculated using Daylight[25] fingerprints to be 0.37 ± 0.07. Virtual screening identified five of eight HERG blockers (62.5%). The three false negatives represent one scaffold (pairwise similarity of 0.94) and contain a pharmacophore closely resembling the 'collapsed' pharmacophore 2 from Table 3. The ring centroids of the two aromatic rings were positioned 4.2 and 4.3 Å from the positively charged nitrogen, slightly out of the range of the pharmacophore bit 2 for F_1F_2 of 4.8–6.7 Å, thus underscoring the potential for improving the model by inclusion of additional compounds in the training set. In addition, two compounds that tested negative in the high throughput assay were flagged as positive in the course of virtual screening. One of those was an analog of a highly HERG active molecule previously confirmed by the patch-clamp method. Since the fluorescence-based assay tends to underestimate the potency of HERG blockers,[26] one or both of the two apparent false positives could potentially represent additional true positives, thus highlighting the potential complementarity of the high throughput HERG binding assays with the virtual screening model described herein. Interestingly, the results of the external validation underscored very good complementarity between the two approaches used in creating the model—of the seven compounds predicted to induce HERG channel blockade four were only identified by 2D screening, while the remaining three were only predicted by the 3D ensemble pharmacophore approach.

An example of a compound identified correctly as a HERG blocker in the course of external validation is a Merck PDE4 inhibitor shown in Figure 6. This molecule does not contain a basic center characteristic of most known HERG blockers, however it was found to be a potent HERG blocker ($IC_{50} = 1\ \mu M$).[27] It was predicted to be a HERG modulator by the VPharm-FP/TOPO/AP model. The prediction was made by a 3–2 vote in the 2D component of the virtual filter, that is, three neighbors were identified in the HERG active dataset. Ketoconazole, loratadine, and mibefradil (Fig. 6) displayed considerable 2D similarity to this inhibitor triggered by the 'fuzzy' atom pairs metric[28] within the TOPO score (see Methods). Indeed, ketoconazole appears to contain topologically similar features to those contained in the PDE4 inhibitor, such as the phenyl group bearing hydrophobic substituents, a benzylic functionality containing a polar group (imidazole vs N-oxide), and a large hydrophobic substituent on the central carbon. Similarity is also apparent between the PDE4 inhibitor and loratadine, with a linker bridging the phenyl and pyridyl moieties in loratadine, and the polar carbamate taking the place of the pyridine N-oxide.

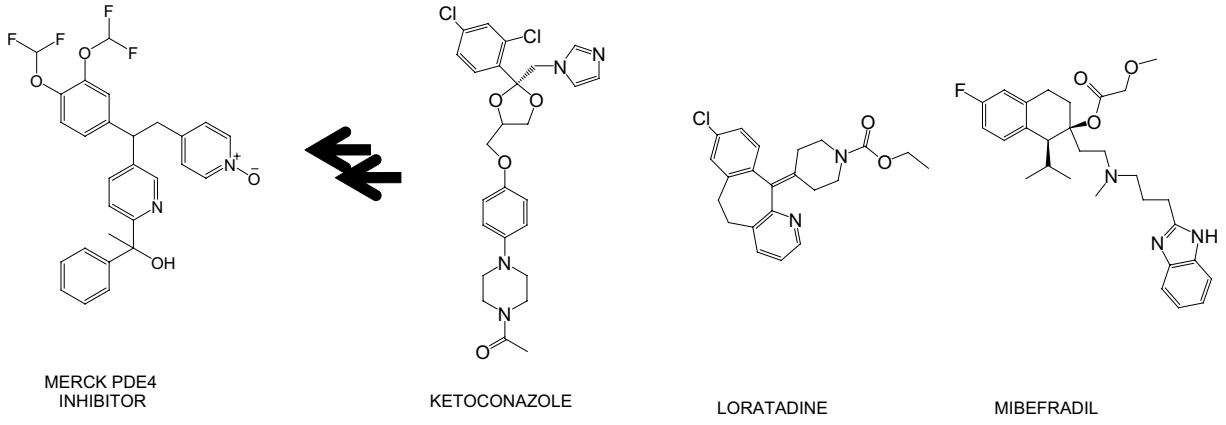

Figure 6. Structures of a Merck PDE4 inhibitor, ketoconazole, loratadine, and mibefradil.

We envision the utility of the HERG classification method primarily in combinatorial library screening. For example, it could be used to flag commercial libraries overly enriched with predicted HERG blockers. Screening virtual libraries used in the course of structure-based ligand design would block compounds with potential QT liabilities from being prepared in the lab. A predicted HERG interaction hit rate would in a sense be a predictive measure of scaffold-related QT prolongation effect. A library containing few predicted positives suggests that the scaffold does not intrinsically contain the structural elements compatible with HERG blockade, and the hit rate may be attributed to substituent effects. However, a high predicted hit rate would be pointing to potential problems within the fixed core. While we feel that the noise level for predicting HERG blocking propensity for a given individual molecule would be too high to permit the use of this model as a predictive tool in the context of a medicinal chemistry optimization program, it will be sufficient to permit in silico identification of potential scaffold-based QT liabilities in the course of whole library screens. Each library, as a consequence, could be described by a statistical distribution of qualifier values, and scaffold selection would be based on the comparison between the different library distributions.[12,29] This application of the method would require its use in conjunction with existing in vitro methods for experimental validation of HERG blockade before a decision regarding the scaffold in question can be made.

3. Conclusions

In conclusion, we have developed a tool for rapid virtual screening of compound libraries for molecules with a potential for QT prolongation. The model combines an ensemble of pharmacophores predicted to capture various chemotypes present among HERG channel blockers with a topological similarity screen that flags molecules with high structural similarity to known QT-prolonging compounds. Since the efforts to obtain larger databases of HERG channel blockers characterized under the same set of reproducible and reliable conditions are currently underway, we see this tool as a step in the direction of being able to predict HERG K^+ channel blocking activity in silico based on molecular structure. There is little doubt that the predictive ability of this approach would benefit from having these larger improved datasets. We expect this model to be useful in conjunction with experimental methods for filtering likely HERG blockers from chemical libraries and virtual chemical databases.

4. Methods

4.1. Dataset description

Using the combined sets of known HERG channel inhibitors assembled by Recanatini and co-workers,[10] Ekins et al.,[9] and Fenichel[30] as a starting point, we updated the collection with a subset of 34 compounds shown to induce HERG blockade in recent publications.[8,9,15,31–47] The list of actives also included class III antiarrhythmic drugs as some of the most potent HERG inhibitors known, and spanned over five orders of magnitude in binding affinity. We chose a reasonable cutoff of 40 μM as a threshold above which effect on HERG activity would not typically be considered clinically relevant. This threshold would likely result in a safety window between physiologically relevant concentrations of most small molecule drugs (with antibiotics and pain medications among the notable exceptions) and potential drug-induced HERG blockade. Depending on the needs of a specific project, this limit can be adjusted, for example, Buyck et al. opted for a significantly lower $pIC_{50} > 6.9$ (130 nM) as a cutoff.[11] The use of the 40 μM cutoff eliminated eight compounds. The remaining 85 compounds active in the HERG assay were used in model building. Since the goal was to create a qualitative virtual screen as opposed to a quantitative model for predicting HERG inhibition, compounds assayed in HERG-transfected non-mammalian cell lines, such as *Xenopus laevis* oocytes, could be kept as part of the set of actives. The highly lipophilic environment in

Xenopus oocytes limits access of the drug to its site of action, leading to a significant underestimation of a drug's potency as a HERG channel blocker,[48,49] however, due to the binary nature of our classification scheme the approach chosen herein is significantly less sensitive to errors of this type. The list of HERG inactives was taken from the recently created in-house database called PILLS.[50] This database contains 486 orally delivered drugs, which were obtained by extracting all orally delivered drugs listed in the 2001 edition of the PDR® Electronic Library.[51] Of these, 367 compounds were left after removing members of unusual classes, such as antifungals, antibacterials, antihelmintics, immunosuppresants, prodrugs, steroids, etc. Known HERG channel inhibitors as well as drugs associated with reports of QT prolongation based on warning labels and adverse effects cited in the literature were removed from the dataset. The remaining 329 compounds formed the set of HERG inactives. Distribution analysis for properties such as molecular weight and a number of rotatable bonds among the HERG actives and inactives is shown in Figures 1 and 2, respectively. While the flexibility distribution for the two subsets was similar, the HERG inactives appeared to have a somewhat lower molecular weight, however this difference is not expected to strongly influence the computational results.

A hold-out data set was randomly selected to represent ~20% of the entire data (83 compounds). This selection was performed 50 times in a random manner. In order to evaluate the predictability and robustness of the classification methods described, the methods described below were tested by performing 50-fold cross-validation on 20% hold-out sets, with the average predictive statistics (see Table 1) summarizing the results.

4.2. 3D pharmacophore fingerprint model

Our pharmacophore fingerprinting and classification system is based on the work of Bradley et al.[20] An in-house program called VPharm-FP was used to construct binary fingerprints that represent the three and four-point pharmacophores contained within the conformational model of a molecule. Each 'bit' in the fingerprint represents a particular pharmacophore that consists of between three and four of the following features: H-acceptor, H-donor, positive, negative, ring, and hydrophobe, along with their associated distance ranges. To construct the fingerprint, the conformational model of each input molecule was created with the program Omega.[52] Next, an individual bit in the fingerprint for a particular molecule is turned on if the pharmacophore represented by that bit is contained within the conformational model of the molecule. After signatures have been created for all the molecules, the individual pharmacophores represented within the signatures were ranked by their information content, that is, their ability to discriminate between active and inactive molecules.[20] An ensemble pharmacophore classification model is then created by selecting the top N pharmacophores from the ranked list. Classification of a molecule is accomplished by calculating a score that is the summation of the information contents of the pharmacophores contained within both the ensemble model and the conformational model of the molecule.

We initially set out to define the optimal number of pharmacophore bits used to build a model (N_{top}). Separate runs generating between 50 and 300 hypotheses were performed in increments of 50 on the entire dataset for both HERG actives and inactives, and the difference between the two sets [(% true positives) – (% false positives)] was used to analyze the quality of the model (data not shown). As a result, $N_{top} = 50$ was chosen for cross-validation. Hypotheses with the highest information content for the entire dataset were assessed based on their performance in the cross-validation experiments.

4.3. 2D topology model

We chose a two-dimensional similarity method coupled with a nearest neighbors-type classification scheme as the first predictive filter for potential HERG-small molecule interactions. The method relied on an in-house program called Multisim to report similarity scores for every molecule in the hold-out set. These scores included four similarity metrics—topological torsions (TT),[22] atom pairs (AP),[23] 'fuzzy' topological torsions,[28] and 'fuzzy' atom pairs;[28] the highest numerical value was considered as descriptive of overall similarity for every molecular pair ('best of' procedure, referred to herein as TOPO). Alternatively, similarity search was performed using only one of the four metrics in Multisim or an in-house implementation of Schneider's CAT similarity.[24] The top five nearest neighbor molecules in each case would then 'vote' to determine the prediction for the HERG-binding character of the test molecule. When used in combination with the pharmacophore filter, the program would classify a molecule as being HERG active if either pharmacophore or topology model labeled it as likely to inhibit HERG ('veto' format).

4.4. Decision tree model

The model was implemented as described in Buyck et al.[11] (see Introduction). ACD pK_a DB was used to predict pK_a values.[53] The model's performance on the entire dataset was assessed.

Acknowledgements

We wish to thank Mark Murcko, John Thomson, Patrick Walters, Peter Grootenhuis, and Guy Bemis for helpful comments on the manuscript. We are also grateful to Gregor Zlokarnik for providing the external validation set and useful discussions, as well as Bill Egan for help with implementation of the decision tree model.

References and notes

1. Keating, M. T.; Sanguinetti, M. C. Molecular genetic insights into cardiovascular disease. *Science* **1996**, *272*, 681–685.
2. Viskin, S. Long QT syndromes and torsade de pointes. *Lancet* **1999**, *354*, 1625–1633.
3. Crumb, W.; Cavero, I. QT interval prolongation by non-cardiovascular drugs: issues and solutions for novel drug development. *Pharm. Sci. Technol. Today* **1999**, *2*, 270–280.
4. Trudeau, M.; Warmke, J. W.; Ganetzky, B.; Robertson, G. A. HERG, a human inward rectifier in the voltage-gated potassium channel family. *Science* **1995**, *269*, 92–95.
5. Sanguinetti, M. C.; Jiang, C.; Curran, M. E.; Keating, M. T. A mechanistic link between an inherited and an acquired cardiac arrhythmia: HERG encodes the IKr potassium channel. *Cell* **1995**, *81*, 299–307.
6. Roti Roti, E. C.; Myers, C. D.; Ayers, R. A.; Boatman, D. E.; Delfosse, S. A., et al. Interaction with GM130 during HERG ion channel trafficking. Disruption by type 2 congenital long QT syndrome mutations. *J. Biol. Chem.* **2002**, *277*, 47779–47785.
7. Paulussen, A.; Raes, A.; Matthijs, G.; Snyders, D. J.; Cohen, N.; Aerssens, J. A novel mutation (T65P) in the PAS domain of the human potassium channel HERG results in the long QT syndrome by trafficking deficiency. *J. Biol. Chem.* **2002**, *277*, 48610–48616.
8. De Ponti, F.; Poluzzi, E.; Cavalli, A.; Recanatini, M.; Montanaro, N. Safety of non-antiarrhythmic drugs that prolong the QT interval or induce torsades de pointes: an overview. *Drug Saf.* **2002**, *25*, 263–286.
9. Ekins, S.; Crumb, W. J.; Sarazan, R. D.; Wikel, J. H.; Wrighton, S. A. Three-dimensional quantitative structure-activity relationship for inhibition of human ether-a-go-go-related gene potassium channel. *J. Pharmacol. Exp. Ther.* **2002**, *301*, 427–434.
10. Cavalli, A.; Poluzzi, E.; De Ponti, F.; Recanatini, M. Toward a pharmacophore for drugs inducing the long QT syndrome: insights from a CoMFA study of HERG K^+ channel blockers. *J. Med. Chem.* **2002**, *45*, 3844–3853.
11. Buyck, C.; Tollenaere, J.; Engels, M.; De Clerck, F. An in silico model for detecting potential hERG blocking. *The 14th European Symposium on Quantitative Structure–Activity Relationships*, 8–13 September 2002; Bournemouth, UK.
12. Roche, O.; Trube, G.; Zuegge, J.; Pflimlin, P.; Alanine, A.; Schneider, G. A virtual screening method for prediction of the hERG potassium channel liability of compound libraries. *ChemBioChem.* **2002**, *3*, 455–459.
13. Pearlstein, R.; Vaz, R.; Rampe, D. Understanding the structure–activity relationship of the human ether-a-go-go-related gene cardiac K^+ channel. A model for bad behavior. *J. Med. Chem.* **2003**, *46*, 2017–2022.
14. Pearlstein, R. A.; Vaz, R. J.; Kang, J.; Chen, X.-L.; Preobrazhenskaya, M.; Shchekotikhin, A. E.; Korolev, A. M.; Lysenkova, L. N.; Miroshnikova, O. V.; Hendrix, J.; Rampe, D. Characterization of HERG potassium channel inhibition using CoMSiA 3D QSAR and homology modeling approaches. *Bioorg. Med. Chem. Lett.* **2003**, *13*, 1829–1835.
15. Mitcheson, J. S.; Chen, J.; Lin, M.; Culberson, C.; Sanguinetti, M. C. A structural basis for drug-induced long QT syndrome. *Proc. Natl. Acad. Sci.* **2000**, *97*, 12329–12333.
16. Lees-Miller, J. P.; Duan, Y.; Teng, G. Q.; Duff, H. J. Molecular determinant of high-affinity dofetilide binding to HERG1 expressed in Xenopus oocytes: involvement of S6 sites. *Mol. Pharmacol.* **2000**, *57*, 367–374.
17. Chen, J.; Seebohm, G.; Sanguinetti, M. C. Position of aromatic residues in the S6 domain, not inactivation, dictates cisapride sensitivity of HERG and eag potassium channels. *Proc. Natl. Acad. Sci.* **2002**, *99*, 12461–12466.
18. Doyle, D. A.; Morais Cabral, J.; Pfuetzner, R. A.; Kuo, A.; Gulbis, J. M.; Cohen, S. L.; Chait, B. T.; MacKinnon, R. The structure of the potassium channel: molecular basis of K+ conduction and selectivity. *Science* **1998**, *280*, 69–77.
19. Mason, J. S.; Good, A. C.; Martin, E. J. 3-D pharmacophores in drug discovery. *Curr. Pharm. Des.* **2001**, *7*, 567–597.
20. Bradley, E. K.; Beroza, P.; Penzotti, J. E.; Grootenhuis, P. D.; Spellmeyer, D. C.; Miller, J. L. A rapid computational method for lead evolution: description and application to alpha (1)-adrenergic antagonists. *J. Med. Chem.* **2000**, *43*, 2770–2774.
21. Penzotti, J. E.; Lamb, M. L.; Evensen, E.; Grootenhuis, P. D. A computational ensemble pharmacophore model for identifying substrates of P-glycoprotein. *J. Med. Chem.* **2002**, *45*, 1737–1740.
22. Nilakantan, R.; Bauman, N.; Dixon, J. S.; Venkataraghavan, R. Topological torsions: a new molecular descriptor for sar applications. Comparison with other descriptors. *J. Chem. Inf. Comput. Sci.* **1987**, *27*, 82–85.
23. Carhart, R. E.; Smith, D. H.; Venkataraghavan, R. Atom pairs as molecular features in structure–activity studies: definition and application. *J. Chem. Inf. Comput. Sci.* **1985**, *25*, 64–73.
24. Schneider, G.; Neidhart, W.; Giller, T.; Schmid, G. 'Scaffold-hopping' by topological pharmacophore search: a contribution to virtual screening. *Angew. Chem., Int. Ed.* **1999**, *38*, 2894–2896.
25. *Daylight Chemical Information Software*; Daylight Chemical Information: Mission Viejo, CA.
26. Zlokarnik, G. Vertex Pharmaceuticals, personal communication, 2003.
27. Friesen, R. W.; Ducharme, Y.; Ball, R. G.; Blouin, M.; Boulet, L.; Cote, B.; Frenette, R.; Girard, M.; Guay, D.; Huang, Z., et al. Optimization of a tertiary alcohol series of phosphodiesterase-4 (PDE4) inhibitors: structure–activity relationship related to PDE4 inhibition and human ether-a-go-go related gene potassium channel binding activity. *J. Med. Chem.* **2003**, *46*, 2413–2426.
28. Kearsley, S. K.; Sallamack, S.; Fluder, E. M.; Andose, J. D.; Mosley, R. T.; Sheridan, R. P. Chemical similarity using physiochemical property descriptors. *J. Chem. Inf. Comput. Sci.* **1996**, *36*, 118–127.
29. Schneider, G. Trends in virtual combinatorial library design. *Curr. Med. Chem.* **2002**, *9*, 2095–2101.
30. Fenichel, R. R. http://fenichel.net/pages/Professional/subpages/QT/Tables/pbydrug.htm
31. Paul, A. A.; Witchel, H. J.; Hancox, J. C. Inhibition of the current of heterologously expressed HERG potassium channels by flecainide and comparison with quinidine, propafenone, and lignocaine. *Br. J. Pharmacol.* **2002**, *136*, 717–729.
32. Volberg, W. A.; Koci, B. J.; Su, W.; Lin, J.; Zhou, J. Blockade of human cardiac potassium channel human ether-a-go-go-related gene (HERG) by macrolide antibiotics. *J. Pharmacol. Exp. Ther.* **2002**, *302*, 320–327.
33. Witchel, H. J.; Pabbathi, V. K.; Hofmann, G.; Paul, A. A.; Hancox, J. C. Inhibitory actions of the selective serotonin re-uptake inhibitor citalopram on HERG and ventricular L-type calcium currents. *FEBS Lett.* **2002**, *512*, 59–66.
34. Thomas, D.; Gut, B.; Wendt-Nordahl, G.; Kiehn, J. The antidepressant drug fluoxetine is an inhibitor of human ether-a-go-go-related gene (HERG) potassium channels. *J. Pharmacol. Exp. Ther.* **2002**, *300*, 543–548.

35. Paul, A. A.; Leishman, D. J.; Witchel, H. J.; Hancox, J. C. Effects of the class III antiarrhythmic agent dofetilide (UK-68,798) on L-type calcium current from rabbit ventricular myocytes. *J. Pharm. Pharmacol.* **2001**, *53*, 1671–1678.
36. O'Leary, M. E. Inhibition of HERG potassium channels by cocaethylene: a metabolite of cocaine and ethanol. *Cardiovasc. Res.* **2002**, *53*, 59–67.
37. Potet, F.; Bouyssou, T.; Escande, D.; Baro, I. Gastrointestinal prokinetic drugs have different affinity for the human cardiac human ether-a-gogo K (+) channel. *J. Pharmacol. Exp. Ther.* **2001**, *299*, 1007–1012.
38. Kamiya, K.; Mitcheson, J. S.; Yasui, K.; Kodama, I.; Sanguinetti, M. C. Open channel block of HERG K (+) channels by vesnarinone. *Mol. Pharmacol.* **2001**, *60*, 244–253.
39. Shuba, Y. M.; Degtiar, V. E.; Osipenko, V. N.; Naidenov, V. G.; Woosley, R. L. Testosterone-mediated modulation of HERG blockade by proarrhythmic agents. *Biochem. Pharmacol.* **2001**, *62*, 41–49.
40. Karle, C. A.; Kreye, V. A.; Thomas, D.; Rockl, K.; Kathofer, S.; Zhang, W.; Kiehn, J. Antiarrhythmic drug carvedilol inhibits HERG potassium channels. *Cardiovasc. Res.* **2001**, *49*, 361–370.
41. Paul, A. A.; Witchel, H. J.; Hancox, J. C. Inhibition of HERG potassium channel current by the class 1a antiarrhythmic agent disopyramide. *Biochem. Biophys. Res. Commun.* **2001**, *280*, 1243–1250.
42. O'Leary, M. E. Inhibition of human ether-a-go-go potassium channels by cocaine. *Mol. Pharmacol.* **2001**, *59*, 269–277.
43. Gonzalez, T.; Longobardo, M.; Caballero, R.; Delpon, E.; Tamargo, J.; Valenzuela, C. Effects of bupivacaine and a novel local anesthetic, IQB-9302, on human cardiac K+ channels. *J. Pharmacol. Exp. Ther.* **2001**, *296*, 573–583.
44. Taglialatela, M.; Pannaccione, A.; Castaldo, P.; Giorgio, G.; Annunziato, L. Inhibition of HERG1 K(+) channels by the novel second-generation antihistamine mizolastine. *Br. J. Pharmacol.* **2000**, *131*, 1081–1088.
45. Bischoff, U.; Schmidt, C.; Netzer, R.; Pongs, O. Effects of fluoroquinolones on HERG currents. *Eur. J. Pharmacol.* **2000**, *406*, 341–343.
46. Walker, B. D.; Singleton, C. B.; Tie, H.; Bursill, J. A.; Wyse, K. R.; Valenzuela, S. M.; Breit, S. N.; Campbell, T. J. Comparative effects of azimilide and ambasilide on the human ether-a-go-go-related gene (HERG) potassium channel. *Cardiovasc. Res.* **2000**, *48*, 44–58.
47. Kreutner, W.; Hey, J. A.; Chiu, P.; Barnett, A. Preclinical pharmacology of desloratadine, a selective and non-sedating histamine H1 receptor antagonist. Second communication: lack of central nervous system and cardiovascular effects. *Arzneimittelforschung* **2000**, *50*, 441–448.
48. Cavero, I.; Mestre, M.; Guillon, J. M.; Crumb, W. Drugs that prolong QT interval as an unwanted effect: assessing their likelihood of inducing hazardous cardiac dysrhythmias. *Expert Opin. Pharmacother.* **2000**, *1*, 947–973.
49. Netzer, R.; Ebneth, A.; Bischoff, U.; Pongs, O. Screening lead compounds for QT interval prolongation. *Drug Discovery Today* **2001**, *6*, 78–84.
50. Egan, W. J.; Walters, W. P.; Murcko, M. A. Guiding molecules towards drug-likeness. *Curr. Opin. Drug Discov. Devel.* **2002**, *5*, 540–549.
51. *Physicians' Desk Reference*®; Thompson Medical Economics: Montvale, NJ. http://www.pdrel.com.
52. *Omega*; OpenEye Scientific Software: Santa Fe, NM.
53. *ACD/Labs*; Advanced Chemistry Development: Toronto, Canada.